NEUROLOGICAL RESEARCH
https://doi.org/10.1080/01616412.2025.2566230

NLRX1 orchestrates neuronal mitophagy in Alzheimer's Disease: a mechanistic exploration

Baoying Qiu[a,b], Jiajun He[a,b], Shu Li[b,c], Qiaoling Wang[a], Wenhua Feng[a,b], Xiaotong Yu[a,b], Yuanyuan Jia[a], Shuyu Liu[a], Dijin Jiao[a] and Ling Xie[a,b]

[a]Department of Anatomy, School of Basic Medicine, Shenyang Medical College, Shenyang, Liaoning, P. R. China; [b]Liaoning Province Key Laboratory for Phenomics of Human Ethnic Specificity and Critical Illness, Shenyang Medical College, Shenyang, P.R. China; [c]Department of Histology and Embryology, School of Basic Medicine, Shenyang Medical College, Shenyang, Liaoning, P. R. China

ABSTRACT

Background: Mitophagy dysfunction in Alzheimer's Disease (AD) accelerates disease progression, highlighting the need for novel therapeutic targets. Although Nucleotide oligomerization domain – like receptor X1 (NLRX1) regulates mitophagy, its role in AD remains unclear. This study aimed to elucidate NLRX1's function in AD – associated mitophagy and its therapeutic potential.

Methods: APP/PS1 transgenic mice and N2A – SW cells were used to establish AD models. Behavioral assays evaluated cognitive function in APP/PS1 mice, while transmission electron microscopy examined mitochondrial morphology. ELISA measured β - amyloid (Aβ) 1–42 levels, and RT – qPCR and Western blot analyzed NLRX1 and mitophagy – related proteins after manipulating NLRX1 expression

Results: APP/PS1 mice had cognitive impairment, elevated Aβ1–42, and abnormal mitochondrial morphology, with reduced NLRX1 expression. NLRX1 - RNAi worsened mitochondrial function, increased Aβ1–42 and mitochondrial ROS, decreased the LC3B – II/I ratio, and upregulated Cyt – C, HSP60, and TIM23, while NLRX1 overexpression alleviated these effects. Co-immunoprecipitation confirmed NLRX1's interaction with key mitophagy protein.

Conclusion: NLRX1 is a key regulator of neuronal mitophagy in AD, and its down-regulation impairs mitophagy, suggesting it as a potential therapeutic target.

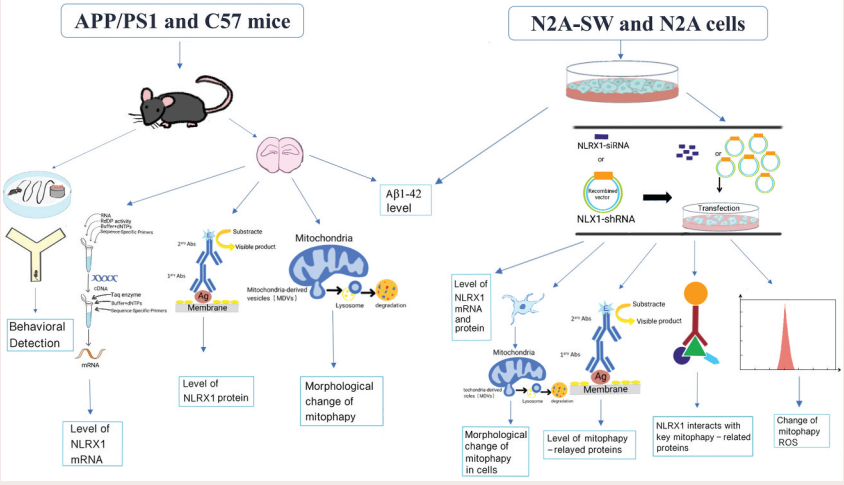

ARTICLE HISTORY
Received 23 May 2025
Accepted 21 September 2025

KEYWORDS
Alzheimer's disease; NLRX1; mitophagy; LC3B; Cyt-c; HSP60; TIM23

1. Introduction

Alzheimer's Disease (AD) is a neurodegenerative disorder characterized by memory loss, cognitive dysfunction, and behavioral abnormalities [1]. AD pathogenesis involves complex and interconnected

CONTACT Ling Xie xieling@symc.edu.cn Department of Anatomy, School of Basic Medicine, Shenyang Medical College, No.146 Huanghe North Street, Yuhong District, Shenyang, Liaoning Province 110034, P. R. China

This article was originally published with error, which have now been corrected in the online version. Please see Correction (http://dx.doi.org/10.1080/01616412.2025.2579424)

processes, including amyloid-β (Aβ) plaque deposition, neurofibrillary tangles formed by hyperphosphorylated tau, neuroinflammation, and synaptic loss. With the intensification of global aging, the incidence of AD continues to rise, making it a major threat to the health of older adults [2]. Epidemiological data indicate that by 2050, the global number of AD patients is projected to exceed 150 million, posing significant challenges to healthcare systems and social resources [3]. Currently, available treatments only provide symptomatic relief without halting or reversing disease progression. Therefore, elucidating the underlying AD pathological mechanisms and identifying novel therapeutic targets are crucial for developing disease-modifying therapies.

Neurons are profoundly dependent on mitochondria for ATP generation via oxidative phosphorylation, as well as for regulating calcium homeostasis, redox balance, mitochondrial dynamics, and apoptosis – processes that are fundamental to neuronal survival and plasticity [4]. Accumulating evidence highlights mitochondrial dysfunction as a central event in AD pathogenesis, which contributes to the cascade of pathological events [5,6]. This dysfunction is now understood to be tightly linked to the failure of mitophagy, a crucial cellular quality control pathway that selectively eliminates damaged mitochondria [7], preventing ROS accumulation and energy failure [8]. When mitophagy is compromised, dysfunctional mitochondria accumulate, amplifying reactive oxygen species and disrupting bioenergetics, thereby exacerbating neurodegeneration [9]. Impaired mitophagy and the pathological changes involving Aβ or Tau may engage in a mutually reinforcing cycle, ultimately resulting in neuronal injury and demise [10]. Consistent with these observations, aging and AD are linked to marked alterations in hippocampal mitochondrial ultrastructure, including reduced length and area, increased fragmentation and swelling, and progressive cristae and membrane deterioration [11]. Thus, restoring mitophagy function has emerged as a promising therapeutic strategy for AD [12].

NLR family member X1 (NLRX1), the only NOD-like receptor reported to localize to mitochondria, has been implicated in the regulation of mitochondrial function, autophagy/mitophagy, and inflammatory signaling [13]. Its unique mitochondrial targeting sequence replacing the effector domain highlights NLRX1's specialized role in coordinating mitochondrial function [14]. Studies indicate that NLRX1 participates in mitophagy initiation by directly interacting with LC3 proteins and maintains mitochondrial homeostasis by regulating mitochondrial membrane potential and cristae morphology [15]. In fields such as central nervous system diseases, ischemia-reperfusion injury, autoimmune disorders, and cancer, NLRX1's regulatory role has garnered significant attention [16], yet its neuroprotective mechanism regarding mitophagy in AD pathogenesis remains unclear. In this study, APP/PS1 transgenic mice and N2A-SW cells were utilized as AD models. Morphological, cell biological, and molecular biological techniques were comprehensively applied to systematically investigate NLRX1 expression changes and its regulatory effects on mitophagy under AD pathological conditions. This study aims to elucidate the molecular mechanisms of NLRX1 in AD-related mitophagy and provide experimental support for developing novel mitophagy-targeted therapeutic strategies for AD.

2. Materials and methods

2.1. Experimental materials

2.1.1. Antibodies and reagents

We obtained antibodies including anti-NLRX1 (Abclonal), anti-LC3B (Abclonal), anti-Hsp60 (Abclonal), anti-Cyt-c (Abclonal), anti-TIM23 (Abclonal), anti-GAPDH (Cell Signaling), anti-α-Tubulin (Cell Signaling), anti-Parkin (Abcam), anti-PINK1 (Abcam), goat anti-rabbit secondary antibody (Gene Tex), and goat anti-mouse secondary antibody (Gene Tex). We obtained reagents including Mouse Aβ1–42 ELISA Kit (Enzyme-linked Biotechnology); Fetal bovine serum (FBS, KeyGen Biotech); DMEM high-glucose medium (Corning); G418 (Genview); FastPure® Cell/Tissue Total RNA Isolation Kit, HiScript® II Q RT SuperMix for qPCR (+gDNA wiper), ChamQ Universal SYBR qPCR Master Mix kit, One Step Mouse Cat.PD101–01 (Novozam, Nanjing, China). The transfection reagent Lipofectamine 2000 was purchased from Invitrogen. The plasmid encoding NLRX1 was provided by SYNBIOTECHNOLOGIES. The siRNA sequence targeting NLRX1 was designed based on GenBank information and synthesized by SYNBIOTECHNOLOGIES. The sequences of small interfering RNA (siRNA) were as follows: siNLRX1–1 5′- UAAGACCAUCUUCCGUACCTT-3′ and siNLRX1–2 5′-UUGAAUCAGGUUGUCGCGCTT –3′.

2.1.2. Animal

Six 6-month-old male APP/PS1 transgenic mice and six male wild-type (WT) mice, all with a C57BL/6J genetic background (Beijing Huafukang Biotechnology Co., Ltd., Production License No.: SCXK (Jing) 2019–0008), were used as animal models for AD. All experimental animals were housed in the SPF-level animal laboratory at Shenyang Medical College under environmental conditions of 22–25°C temperature, 50% relative humidity, and a 12-hour light/dark cycle. The experiments strictly adhered to ethical and welfare principles for laboratory animals. Genotyping of the mice was performed using PCR with the following primers: forward primer, AGGACTGACCACTCGACCAG; reverse primer, CGGGGGTCTAGTTCTGCAT. Animal experiments were approved by the Animal Experiment Ethics Committee of Shenyang Medical College (No. SYYXY2023111201).

2.1.3. Cell culture

The mouse neuroblastoma cells (N2A) and their stable transfection clone carrying the APP695 Swedish mutation gene (N2a-SW cells), kindly provided by Associate Professor Huiling Gao of Northeastern University, were cultured following standardized protocols for AD cell models. The base culture medium consisted of 95% DMEM high-glucose medium (Corning), 5% fetal bovine serum (FBS, KGI Biotechnology), 100 units/mL penicillin, and 100 μg/mL streptomycin. For N2a-SW cells, the medium was supplemented with 200 μg/mL G418 (Genview) to maintain selection pressure. All cells were routinely maintained in a humidified incubator at 37°C with 5% CO_2.

2.2. Experimental methods

2.2.1. Animal behavioral tests

This study utilized the Morris water maze (MWM) and Y-maze spontaneous alternation test to assess spatial learning and memory in experimental animals.

The MWM was performed over 8 consecutive days following a modified protocol established by our group (Guo et al., Neurobiol Aging, 2013; Guo et al., Neurochem Int, 2013), utilizing a circular pool (100 cm diameter, 50 cm height) filled with water (23–25°C) divided into four quadrants, with a hidden platform (10 cm diameter, 30 cm height) placed in one quadrant. During the 5-day acquisition phase, animals received four daily training trials with 15-minute intervals, starting from different positions. Escape latency and swimming paths were recorded. The platform was visible for 2 days and submerged 1 cm below the surface for the remaining 3 days. In the spatial probe test, with the platform removed, animals were released from a novel position, and time spent in the target quadrant and platform crossings were measured.

The test consisted of three phases:

Days 1–2 (Visible platform training): The platform was positioned above the water surface to habituate mice to the task. Each mouse underwent four daily trials (randomized release from four quadrants, 15 min inter-trial interval); those failing to find the platform within 60 s were guided to it and allowed to remain for 10 s.

Days 3–7 (Hidden platform acquisition): The platform was submerged 1 cm below the water surface, with escape latency recorded from Day 3 to assess spatial learning.

Day 8 (Probe trial): The platform was removed, and mice swam freely for 60 s; the number of platform crossings and time spent in the target quadrant were recorded to evaluate memory retention.

During the 5-day acquisition phase (encompassed in Days 1–7), four daily training trials (15 min intervals, varied starting positions) were conducted, with escape latency and swimming paths recorded. The Y-maze, composed of three 120°-angled, 30-cm-long, 6-cm-wide, 15-cm-high arms with smooth, unmarked walls, was used to evaluate working memory via spontaneous alternation rate. Mice were first allowed 5 minutes for environmental adaptation at the maze center, then released from one arm for a 6-minute free exploration. The sequence and total number of arm entries (when all four limbs entered) were recorded. The spontaneous alternation rate was calculated using the following formula: Spontaneous alternation rate = [Number of times of consecutive entry into three different arms/(Total number of arm entries − 2)] × 100%.

2.2.2. ELISA

Aβ1–42 levels were quantified using a Mouse Aβ1–42 ELISA Kit (Abcam, UK) following the manufacturer's protocol. For brain tissues: Mouse brain tissues were homogenized in 0.01 M PBS (pH 7.4) at 1:9 (w/v), centrifuged at 1000 × g for 5 min, and supernatants stored at −80°C. For cell cultures: Cells were seeded to 70% confluency, medium replaced, cultured for 24 h, and supernatants collected by centrifugation at 1000 × g for 5 min. Serially diluted standards (0–500 pg/mL) and samples were added in triplicate to precoated wells ($n = 6$) and incubated for 2 h at room temperature. After washing, biotinylated detection antibody was added (1 h incubation), followed by streptavidin-HRP conjugate (30 min incubation). TMB substrate was added for 15–30 min (room temperature, dark) before reaction termination with stop solution. Absorbance was measured at 450 nm (reference 570 nm) using a microplate reader (Model 680, Bio-Rad, USA). A four-parameter logistic curve derived from standards was used to calculate Aβ1–42 concentrations.

2.2.3. Transmission electron microscopy (TEM)

Freshly dissected mouse prefrontal cortex and hippocampal tissues were immediately cut into 1 mm^3 cross-sectional blocks or the cells were made into a suspension. The samples were fixed with 2.5% glutaraldehyde, and then post-fixed with 1% osmium tetroxide. After dehydration with a gradient of ethanol, they were embedded in epoxy resin. Ultra-thin sections with a thickness of 70 nm were cut, and stained with uranyl acetate and lead citrate. These sections were stained with uranyl acetate and lead citrate. Images were collected using a transmission electron microscope (Hitachi HT7800).

2.2.4. Construction of NLRX1 gene-silenced cell line

Logarithmic-phase N2A cells were seeded at 2×10^5 cells/well in 6-well plates. After 24 h incubation to achieve 70%–80% confluency, transfection was performed. Briefly, 5 μL of siRNA targeting NLRX1 (final 50 nM) or negative control siRNA was mixed with 250 μL of Opti-MEM (Tube A), while 5 μL of Lipofectamine 2000 was added to 250 μL of Opti-MEM and incubated for 5 min (Tube B). Tube A was added to Tube B, mixed gently, and incubated for 20 min to form transfection complexes. Cells were washed with PBS, treated with 500 μL of Opti-MEM containing complexes for 6 h, then refreshed with 2 mL of DMEM supplemented with 10% FBS. NLRX1-silenced N2A cells were established via puromycin selection, and NLRX1 expression was verified by RT-qPCR and Western blot.

2.2.5. Construction of NLRX1-overexpressing cell line

To construct the NLRX1-overexpressing cell line, N2A-SW cells in the logarithmic growth phase were seeded at an appropriate density in a 6-well cell culture plate. When the cell confluence reached approximately 70%-80%, transfection was initiated. According to the manufacturer's instructions for Lipofectamine 2000 reagent, an appropriate amount of plasmid encoding NLRX1 and Lipofectamine 2000 were separately diluted in Opti-MEM medium, gently mixed, and incubated at room temperature for 20 minutes to form a DNA-liposome complex. This complex was then added dropwise to the cell-containing medium, followed by gentle shaking and incubation in a humidified cell incubator at 37°C with 5% CO_2. After 6–8 hours of transfection, the medium was replaced with complete medium, and the cells were cultured for an additional 48–72 hours. The expression level of NLRX1 was verified using RT-qPCR and WB.

2.2.6. RT – qPCR

Hippocampal tissues and cells from each group were collected for RNA. Total RNA was extracted from an RNA extraction kit (Vazyme). From the total RNA, cDNA was synthesized using a cDNA Reverse Transcription Kit (Vazyme). Real time PCR was performed using Real-time PCR System (Vazyme). GAPDH or α-Tubulin, a housekeeping gene, was used for normalization and relative quantification. The corresponding primer sequences are listed in Table 1. The relative expression of NLRX1 was calculated using the 2^{-} ΔΔCt method.

2.2.7. Western blotting

Western Blotting (WB) analyzed NLRX1, LC3B, TIM23, HSP60, and Cyt-C protein levels. Hippocampal tissues and N2A, N2A-SW cell lysates were homogenized in RIPA buffer with inhibitors. Protein concentration was determined by BCA assay (Thermo Fisher Scientific). Equal 30-μg

Table 1. Primer base sequence of RT-qPCR detection.

Gene	Forward primer sequences (5′-3′)	Reverse primer sequences (5′-3′)
NLRX1	GGAGCGAGATCCCTCCAAAAT	GGCTGTTGTCATACTTCTCATGG
α-Tubulin	TGTGGATTCTGTGGAAGGCG	AAGCACACATTGCCACATACAA
GAPDH	GGAGCGAGATCCCTCCAAAAT	GGCTGTTGTCATACTTCTCATGG

samples underwent SDS-PAGE, transferred to PVDF membranes (Millipore). Membranes were blocked with 5% skim milk in TBST for 1 h, incubated with primary antibodies (1:1000) overnight at 4°C, then washed and probed with HRP-conjugated secondary antibodies (1:1000) for 1 h. The membranes were trimmed prior to imaging and presentation. α-tubulin or GAPDH was used as a loading control for normalization. Protein bands were visualized by ECL (Thermo Fisher Scientific) and quantified using Image J software.

2.2.8. Co-immunoprecipitation (co-IP) assay

Briefly, N2A-SW cells were lysed in ice-cold RIPA buffer. The cell lysates were pre-cleared by incubating with Protein A/G agarose beads (Santa Cruz Biotechnology, USA) for 1 h at 4°C with gentle agitation. The supernatants were then incubated overnight at 4°C with the appropriate primary antibodies, as listed in Table 1. After overnight incubation, 30 µL of Protein A/G agarose beads were added to the lysates and incubated for an additional 2 h at 4°C. The beads were washed three times with RIPA buffer to remove non-specifically bound proteins. The immunoprecipitated proteins were eluted with SDS-PAGE sample buffer and analyzed by Western blotting.

2.2.9. ROS detection by flow cytometry

Reactive oxygen species (ROS) levels were detected using 2‘,7’-dichlorodihydrofluorescein diacetate (DCFH-DA, Sigma-Aldrich, USA), a cell-permeable fluorescent probe. Briefly, cells were seeded in 6-well plates at a density of 5×10^5 cells per well and cultured overnight. After respective treatments, the medium was removed, and cells were washed twice with pre-warmed phosphate-buffered saline (PBS, Gibco, USA). Then, DCFH-DA working solution (10 µM, diluted in serum-free medium) was added to each well, and cells were incubated at 37°C in a 5% CO_2 incubator for 30 min in the dark. Following incubation, cells were trypsinized with 0.25% trypsin-EDTA (Gibco, USA) for 2 min, neutralized with complete medium, and centrifuged at 300 × g for 5 min. The supernatant was discarded, and the cell pellet was resuspended in 500 µL of pre-warmed PBS. Fluorescence intensity, which reflects intracellular ROS levels, was immediately measured using a flow cytometer (BD FACSCanto II, BD Biosciences, USA) with excitation at 488 nm and emission at 525 nm. At least 10,000 events were collected per sample, and data were analyzed using FlowJo software (Version 10, FlowJo LLC, USA).

2.2.10. Statistical analysis

All data are presented as mean ± standard deviation (mean ± SD). Statistical analysis was performed using GraphPad Prism software. Normality of the data was assessed using the Shapiro-Wilk test, and homogeneity of variance was tested with Levene’s test. Data that met the assumptions of normality and equal variance were analyzed by one-way ANOVA followed by Tukey’s post-hoc test. For non-normally distributed data the Mann-Whitney U test was used. $p < 0.05$ was considered statistically significant.

3. Results

3.1. Results of behavioral tests

In the Morris water maze test, escape latency data were collected starting from Day 3, after two days of visible platform pre-training. On Day 3, no significant differences between WT and APP/PS1 mice were observed, suggesting minimal cognitive deficits. However, from Day 4, APP/PS1 mice showed significantly prolonged escape latencies compared to WT mice, indicating impaired spatial learning (Figure 1(A), $p < 0.01$). In the probe trial (Day 8), APP/PS1 mice exhibited significantly fewer crossings in Spatial Probe Test (Figure 1(B, D, E, F, G), $p < 0.01$) compared to wild-type mice.

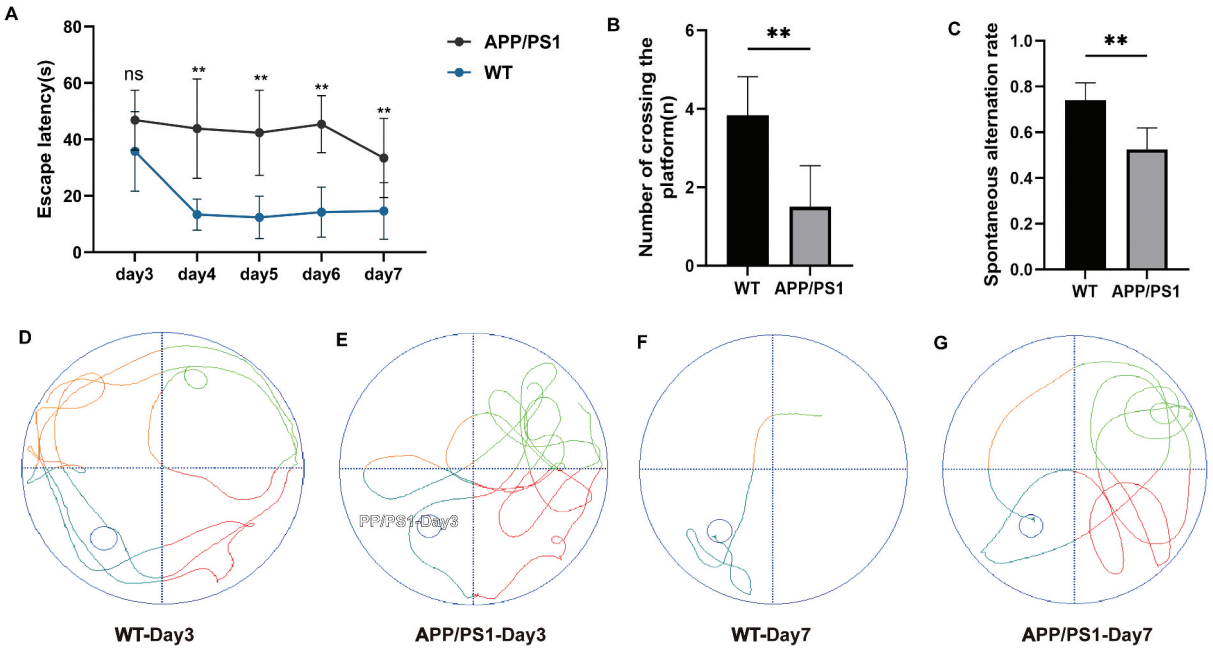

Figure 1. Results of animal behavioral tests. (A) Results of Acquisition Phase Test; (B) Results of Spatial Probe Test; (C) Results of Spontaneous Alternation Test; (D) Acquisition Phase trajectory of WT mice on day 3; (E) Acquisition Phase trajectory of APP/PS1 mice on day 3; F. Acquisition Phase trajectory of WT mice on day 7; G. Acquisition Phase trajectory of APP/PS1 mice on day 7. (**$p < 0.01$).

Additionally, the Y-maze test showed that the spontaneous alternation rate of the APP/PS1 group mice was significantly lower than that of the WT group mice (Figure 1(C), $p < 0.01$). These findings confirm the successful establishment of the AD animal model, with significant impairments in spatial learning and memory.

3.2. Aβ1–42 levels in the brains of APP/PS1 mice

To assess the pathological hallmark of Aβ accumulation in our AD model, we quantified Aβ1–42 levels in cortical tissues of APP/PS1 transgenic mice and wild-type controls using ELISA. Consistent with the well-established phenotype of this model, APP/PS1 mice exhibited significantly higher Aβ1–42 levels (896.1 ± 164.5 pg/mg total protein) compared to WT mice (389.6 ± 224.8 pg/mg; $p < 0.05$) (Figure 2(A)). This ~2.3-fold increase aligns with prior characterizations of the APP/PS1 strain, wherein Radde et al. reported cortical Aβ1–42 levels of 850 ± 190 pg/mg in 6-month-old mice, a critical age for amyloid plaque onset [17]. Similarly, Oblak et al. observed comparable elevations in Aβ1–42 [18], further validating the robustness of this model in mimicking human AD pathology.

3.3. Morphological changes in mitochondria of the frontal cortex and hippocampus in APP/PS1 mice

Next, we assessed neuronal ultrastructural integrity in the frontal cortex and hippocampus of APP/PS1 mice using TEM. The mitochondria in WT mice exhibited intact structures with no swelling and preserved cristae (Figure 2(E, F, I, J)). In contrast, neurons from APP/PS1 mice displayed marked mitochondrial swelling, enlarged volume, disrupted and fragmented cristae, and the presence of autophagosomes or autolysosomes, indicative of impaired mitochondrial integrity and autophagic activation (Figure 2(G, H, K, L)).

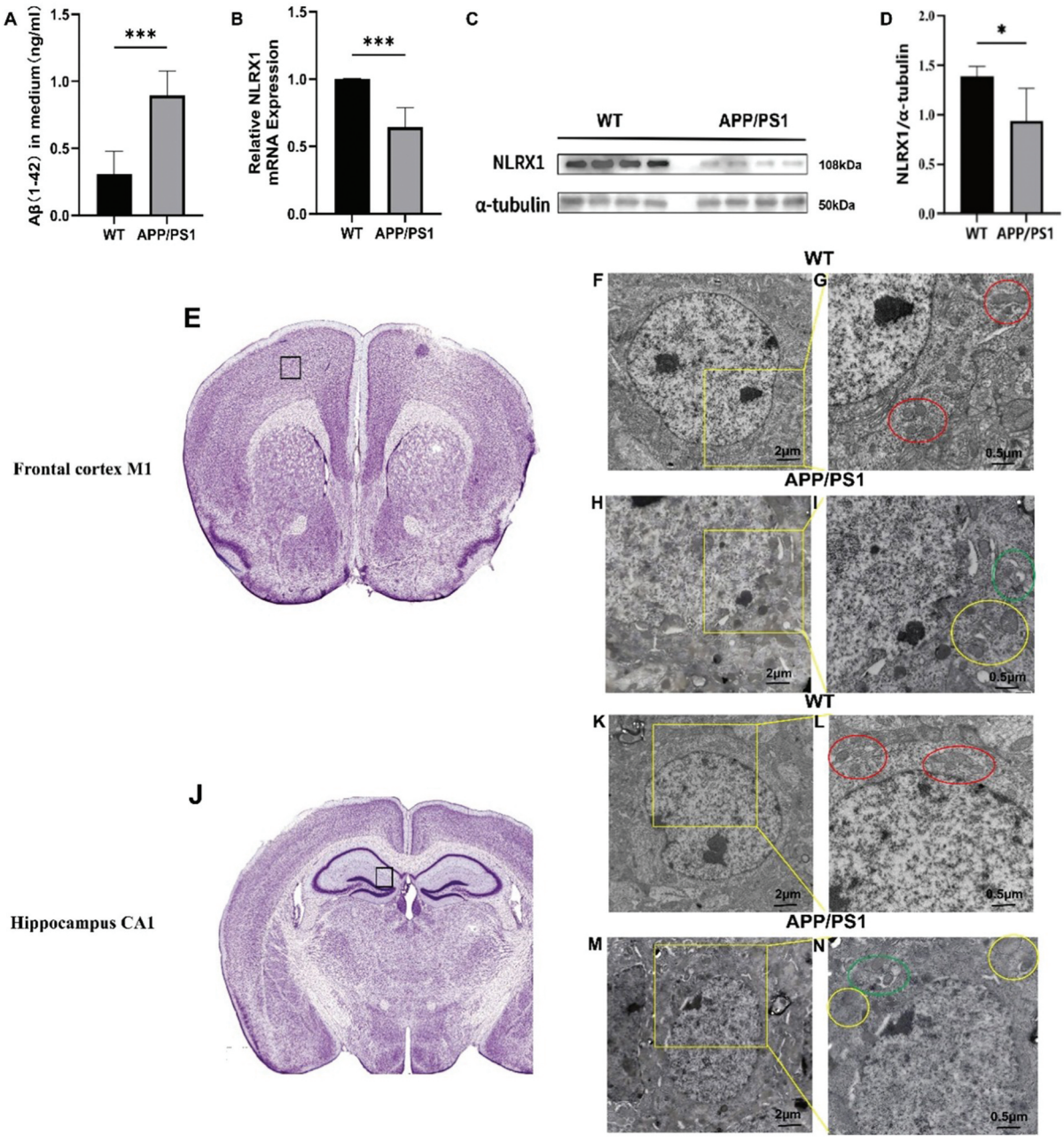

Figure 2. Changes of Aβ1–42, NLRX1 and Mitophagy in brains of APP/PS1 Mice .(A) The level of Aβ1–42 in brains of APP/PS1 Mice; (B) the expression of NLRX1 mRNA in APP/PS1 mice; (C,D) the level of NLRX1 protein in APP/PS1 mice; (E) J. M1 and CA1 regions in Plate Nissl 19 and 43 of mouse brains (ref: PAXINOS AND FRANKLIN'S THE MOUSE BRAIN IN STEREOTAXIC COORDINATES FIFTH EDITION); (F-I) mitochondrial morphology in the M1 region of the frontal cortex of APP/PS1 mice; K-N. mitochondrial morphology in CA1 region of the hippocampus of APP/PS1 Mice (Note: Red circles indicate mitochondria; yellow circles highlight mitochondrial vacuolization, swelling, and cristae disruption; green circles denote autophagosomes or autolysosomes. Black Scale Bars = 2 μm or 0.5 μm. *$p < 0.05$; ***$p < 0.001$).

3.4. NLRX1 expression in the brains of APP/PS1 mice

To investigate the potential involvement of NLRX1 in AD pathogenesis, we systematically analyzed its expression patterns in the brains of APP/PS1 Mice. RT-qPCR results revealed that NLRX1 mRNA levels were significantly decreased in APP/PS1 mice compared to the WT group (in Figure 2(B), $p < 0.001$). Similarly, Western blotting demonstrated a significant reduction in NLRX1 protein expression in APP/PS1 mice (in Figure 2(C, D), $p < 0.05$). These findings position NLRX1 as a novel molecular player in AD pathogenesis.

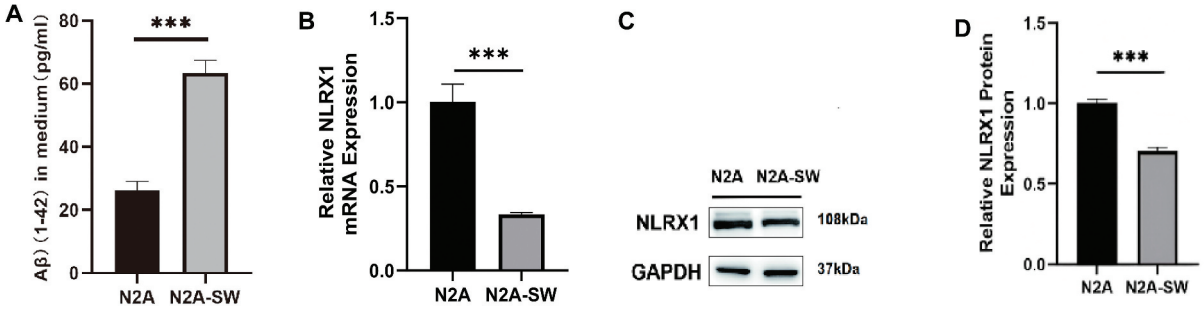

Figure 3. Levels of Aβ1–42 and NLRX1 in N2A-SW Cells. (A) The level of Aβ1–42 in N2A-SW cells; (B) the expression of NLRX1 mRNA in N2A-SW cells; (C, D) the level of NLRX1 protein in N2A-SW cells. (***$p < 0.001$).

3.5. Levels of Aβ1–42 and NLRX1 in N2A-SW cells

We first validated the N2A-SW cell line as a robust in vitro model of amyloid pathology by quantifying extracellular Aβ1–42 secretion using ELISA. As shown in Figure 3(A), Aβ1–42 levels in N2A-SW cells (63.3 ± 3.30 pg/ml) were significantly elevated compared to those in N2A cells (26.0 ± 2.16 pg/ml; $p < 0.001$).This elevation aligns precisely with the established pathogenic phenotype of APPswe mutation, matching previous reports showing 2.3–2.5 fold increases in Aβ1–42 secretion in similar models, as evidenced by Chen et al., who observed ~60 pg/mL Aβ1–42 in N2a.Swe.APP695 cells versus 25 pg/mL in controls [19].

To further investigate the molecular changes associated with AD pathology, we assessed the expression of NLRX1, a gene implicated in cellular stress responses, in both N2A and N2A-SW cells using RT-qPCR and Western blotting. RT-qPCR results (Figure 3(B)) demonstrated that NLRX1 mRNA levels were significantly reduced in N2A-SW cells compared to N2A cells ($p < 0.001$), consistent with observations in animal experiments, indicating downregulation of NLRX1 gene expression under AD pathological conditions. Similarly, Western blotting revealed significantly lower NLRX1 protein levels in N2A-SW cells than in N2A cells ($p < 0.001$, Figure 3(C, D)), further corroborating NLRX1 downregulation in the AD cellular environment.

3.6. Effects of NLRX1 gene overexpression on mitophagy in cells

To investigate the functional consequences of NLRX1 upregulation in AD neuron-associated mitophagy, an NLRX1-overexpressing N2A-SW cell line was constructed. Successful transfection was confirmed by significant increases in both NLRX1 mRNA (Figure 4(A), $p < 0.001$) and protein levels (Figure 4(B) and C, $p < 0.001$) compared to the empty vector group. We then evaluated the impact of NLRX1 overexpression on Aβ1–42 secretion. As shown in Figure 4(D), the Aβ1–42 secretion levels in N2A-SW cells with NLRX1 overexpression (52.7 ± 3.03 pg/ml) were significantly lower than those in the empty vector group (70.7 ± 4.19 pg/ml) ($p < 0.01$), suggesting upregulation of NLRX1 could inhibit Aβ1–42 secretion.

Next, TEM was employed to examine the effects of NLRX1 overexpression on mitochondrial morphology. The mitochondria in N2A-SW cells transfected with the empty vector (NLRX1-NC) exhibited significant swelling, increased volume, and damaged cristae structure (Figure 4(I, J)). In contrast, NLRX1-overexpressing N2A-SW cells showed an increase in the number of mitochondrial autophagosomes and autolysosomes (Figure 4(K, L)), indicating activation of mitophagy. WB analysis further confirmed these observations. The ratio of LC3B-II/LC3B-I, a hallmark of autophagosome formation, was significantly increased in N2A-SW cells with NLRX1 overexpression. In contrast, markers of mitochondrial damage, including Cyt-C, TIM23, and HSP60, were significantly decreased (Figure 4(E, F)).

These results suggest that upregulated NLRX1 expression enhances autophagosome formation and reduces mitochondrial damage in AD models.

3.7. Effects of NLRX1 silencing on mitophagy in cells

To further investigate the role of NLRX1 in mitophagy in AD, we generated NLRX1-silenced N2A cell lines via targeted knockdown of NLRX1 expression. As shown in Figure 5(A), NLRX1-silenced cells exhibited

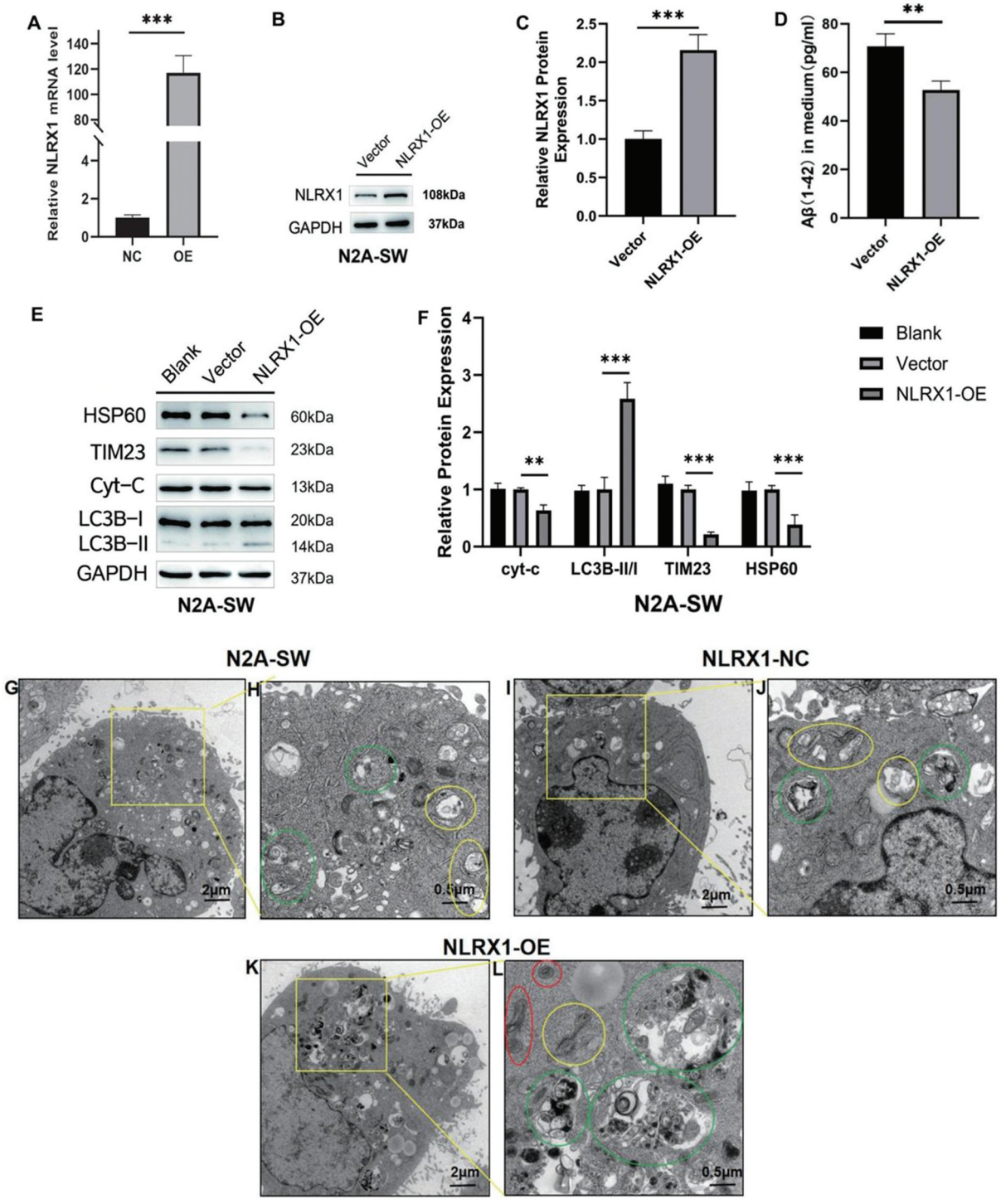

Figure 4. Effects of NLRX1 gene overexpression on mitophagy in cells. (A) The expression of NLRX1 mRNA in cells; (B, C) the level of NLRX1 protein in cells; (D) the level of Aβ1–42 in cells; (E, F) the level of HSP60, TIM23, Cyt-C and LC3B protein in cells; G-L. mitochondrial morphology in cells. (Note: Red circles indicate mitochondria; yellow circles highlight mitochondrial vacuolization, swelling, and cristae disruption; green circles denote autophagosomes or autolysosomes. Scale bars = 2 μm and 0.5 μm (black). $^{**}p < 0.01$; $^{***}p < 0.001$).

significantly reduced NLRX1 mRNA ($p < 0.001$) and protein levels (Figure B and C, $p < 0.01$ or $p < 0.001$) compared to the control group, confirming successful silencing of NLRX1 expression.

ELISA analysis revealed that Aβ1–42 secretion levels in NLRX1-silenced N2A cells (48.5 ± 2.82 pg/ml and 43.8 ± 2.99 pg/ml) were significantly elevated compared with the control value (31.3 ± 1.36 pg/ml) (Figure 5(D)),

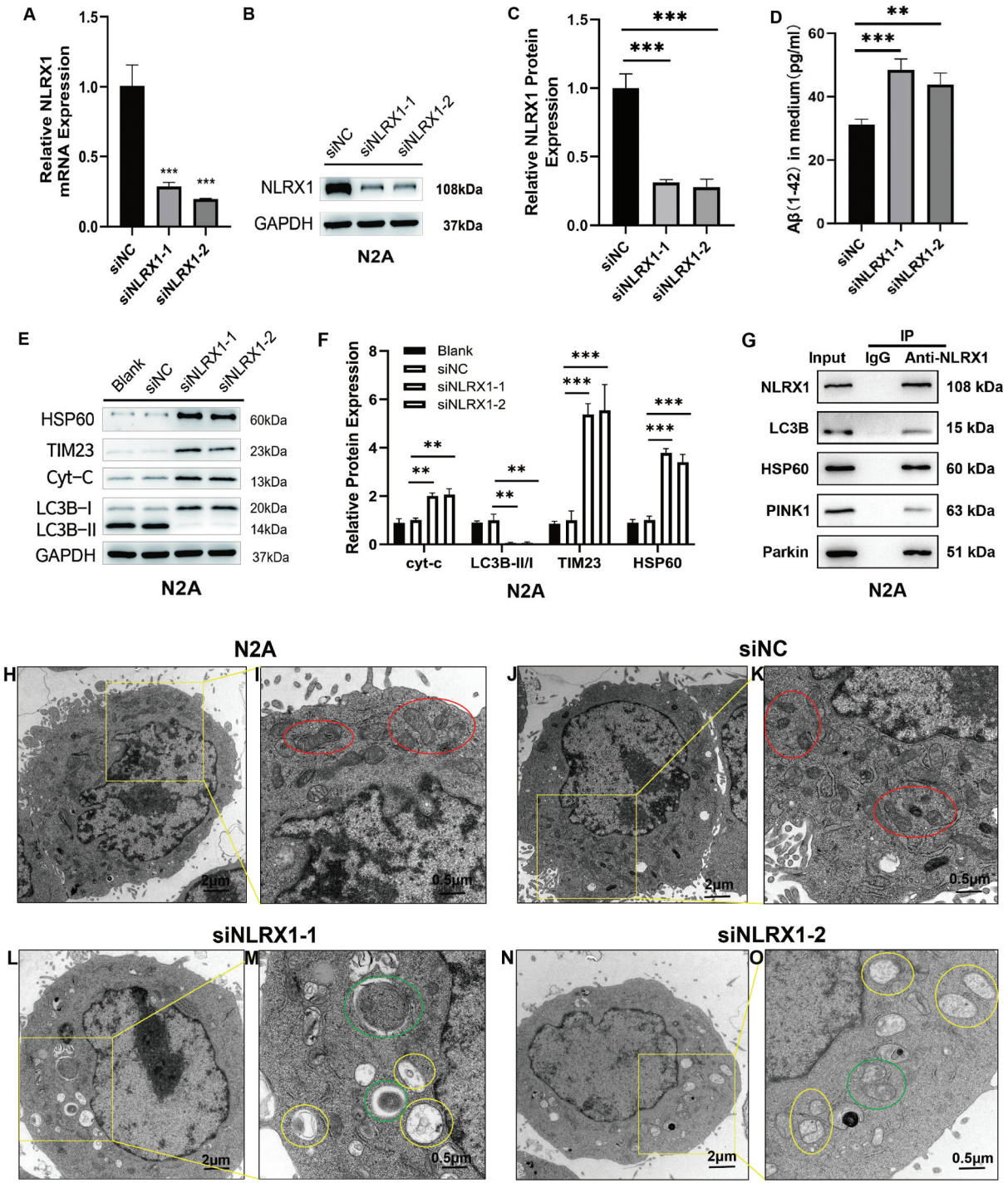

Figure 5. Effects of NLRX1 gene silencing on cellular mitophagy. (A) The expression of NLRX1 mRNA in cells; (B, C) the level of NLRX1 protein in cells; (D) the level of Aβ1–42 in cells; (E, F) the level of HSP60, TIM23, Cyt-C and LC3B protein in cells; G, Co-IP experiments in N2A cells revealed that NLRX1 interacts with key mitophagy-related proteins. H-O. mitochondrial morphology in cells. (Note: Red circles represent mitochondria, yellow circles indicate mitochondrial vacuolization, swelling, and cristae destruction, green circles denote autophagosomes or autolysosomes, black scale bars = 2 μm and 0.5 μm. $^{**}p < 0.01$; $^{***}p < 0.001$).

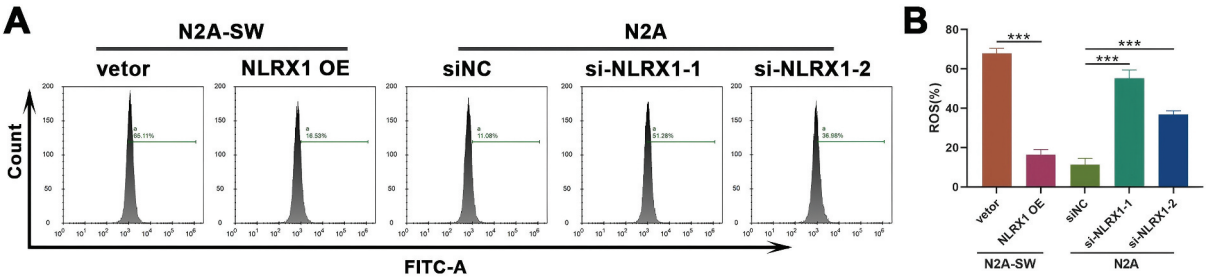

Figure 6. NLRX1 regulates mitochondrial ROS levels in neuronal cells. (A) Flow cytometry analysis of mitochondrial ROS in N2A-SW cells transfected with NLRX1 plasmid or empty vector. (B) Flow cytometry analysis of mitochondrial ROS in N2A cells transfected with si-NLRX1–1, si-NLRX1–2 or scramble control. Quantitative analysis is shown on the right. ***$p < 0.001$.

indicating that NLRX1 downregulation exacerbates Aβ1–42 secretion. TEM analysis demonstrated severe mitochondrial abnormalities in NLRX1-silenced cells, including swollen mitochondria, enlarged volumes, and disrupted/sparse cristae (Figure 5(K, L, M, N)), suggesting impaired mitophagy.

WB further confirmed the effects of NLRX1 silencing on autophagy and mitochondrial integrity. The LC3B-II/LC3B-I ratio. was significantly decreased in NLRX1-silenced cells (Figure 5(E) and (F), $p < 0.01$), indicating a reduction in autophagic activity. In contrast, mitochondrial damage markers, including Cyt-C, TIM23, and HSP60, were significantly elevated ($p < 0.01$ or $p < 0.001$, Figure 5(E, F)), suggesting that NLRX1 silencing leads to increased mitochondrial damage. Co-IP experiments in N2A cells revealed that NLRX1 interacts with key mitophagy-related proteins, including LC3B, HSP60, PINK1, and Parkin (Figure 5(G)).

Taken together, these results demonstrate that NLRX1 downregulation reduces autophagosome formation and exacerbates mitochondrial damage.

3.8. NLRX1 modulates mitochondrial ROS production in neuronal cells

To validate the mechanistic role of NLRX1 in regulating mitochondrial oxidative stress, we directly measured mitochondrial ROS levels using flow cytometry under conditions of NLRX1 overexpression and knockdown. In N2A-SW cells, overexpression of NLRX1 significantly reduced mitochondrial ROS levels compared to the vector control group ($p < 0.001$, Figure 6(A)). In contrast, silencing of NLRX1 in N2A cells led to a marked increase in mitochondrial ROS levels compared to the scramble control ($p < 0.001$ for si-NLRX1–1 and si-NLRX1–2, Figure 6(B)). Collectively, these results provide direct experimental evidence that NLRX1 negatively regulates mitochondrial ROS production, supporting its proposed role in mitigating mitochondrial oxidative stress in neuronal cells

4. Discussion

AD is a chronic, progressive neurodegenerative disorder that primarily impairs cognitive function in the elderly [1–3]. Mitophagy, as a key process for cells to eliminate damaged mitochondria, has been considered to play an important role in the pathological development of AD [20]. In this study, we observed reduced NLRX1 expression in the frontal cortex and hippocampus of APP/PS1 mice, coincident with pronounced mitochondrial ultrastructural abnormalities and cognitive impairment. In complementary cell systems, NLRX1 downregulation was associated with impaired mitophagy and increased Aβ1–42 levels, whereas NLRX1 overexpression enhanced mitophagy readouts and lowered Aβ burden. Together, these findings support a model in which NLRX1 helps preserve mitochondrial integrity under AD-like stress, and its loss contributes to defective mitophagy and exacerbated amyloid pathology.

Mitophagy is indispensable for neuronal homeostasis, as it removes dysfunctional mitochondria to prevent ROS accumulation and energy failure [21,22]. Importantly, when the function of mitophagy is blocked, the neuroprotective function of neurons is weakened, and significant dysfunctions such as abnormal mitochondrial transport and dynamics occur, which also leads to the exacerbation of AD pathological changes [5,7]. In AD, mitophagy impairment exacerbates Aβ deposition, synaptic loss, and

neurodegeneration [12,23], yet the upstream regulators of this process are poorly understood. In this study, decreased NLRX1 mRNA and protein in APP/PS1 neurons, alongside mitochondrial changes, suggests a strong link between NLRX1 downregulation and AD-related mitochondrial pathology.

NLRX1, a mitochondria-localized NOD-like receptor, regulates intracellular immune responses and mitochondrial function [24]. In recent years, it has been confirmed that NLRX1 affects the level of mitophagy in tumor cells [25]. However, to date, no primary research has directly investigated the role of NLRX1 in mitophagy within the context of Alzheimer's disease pathology [26]. In this study, our findings demonstrated that NLRX1 expression is significantly decreased in both AD animal and cellular models. Functional experiments revealed that loss of NLRX1 was associated with diminished mitophagy readouts and higher Aβ1–42. Conversely, when the NLRX1 gene was overexpressed, a marked increase in mitochondrial autophagosomes was noted, indicating enhanced mitophagy [4]. These findings confirm that NLRX1 plays a regulatory role in AD mitophagy.

LC3B is a subtype of the LC3 protein family, encoded by the MAP1LC3B gene, and is a protein related to cellular autophagy, playing a key role in the process of cellular autophagy [26,27]. During autophagy activation, LC3B-I (unmodified form) will be converted into LC3B-II (modified form), a process essential for autophagosome encapsulation of damaged mitochondria and a key marker of autophagosome formation [28]. In this study, NLRX1 overexpression increased LC3B-II/LC3B-I ratios (a hallmark of autophagosome formation) and promoted mitochondrial autophagosomes, while silencing had the opposite effect – confirming NLRX1 drives neural mitophagy via LC3B lipidation. This aligns with NLRX1's role in regulating mitophagic flux, likely through direct modulation of LC3 lipidation during mitochondrial stress [13]. Additionally, NLRX1 maintains mitochondrial membrane potential ($\Delta\Psi m$) and suppresses ROS – critical for stabilizing PINK1 and activating Parkin [29]. In AD pathogenesis, ROS bursts may disrupt these processes, abrogating Parkin-mediated LC3B lipidation [8]. NLRX1 deficiency may further impair PINK1/Parkin pathway function, compromising LC3B-dependent autophagosome formation – a mechanism consistent with our observed changes in LC3B-II/I ratios [28,29]. In this study, we found that silencing the NLRX1 gene increased the level of Cyt-C, whereas overexpression of NLRX1 decreased Cyt-C expression, implying a potential regulatory role of NLRX1 in maintaining mitochondrial integrity through mitophagy. TIM23 serves as a protein transport channel on the inner mitochondrial membrane, primarily responsible for importing nuclear-encoded mitochondrial precursor proteins into the mitochondrial matrix [30,31]. Although TIM23 does not directly participate in mitophagy, it plays a pivotal role in preserving mitochondrial structure and function. When mitochondria are damaged, TIM23 function may be impaired, leading to mitochondrial internal environmental imbalance and subsequently triggering mitophagy. In this study, NLRX1 silencing paradoxically increased TIM23 levels, potentially due to the retention of abnormal mitochondria caused by autophagy deficiency. NLRX1 May maintain TIM23 structural stability by inhibiting ROS production, indirectly ensuring mitochondrial functionality. HSP60 is a mitochondrial heat shock protein that assists in the correct folding and assembly of mitochondrial polypeptide chains, thereby ensuring protein stability and functionality, which is crucial for maintaining mitochondrial metabolism and homeostasis [32]. During mitophagy activation, HSP60 levels often change, reflecting mitochondrial internal environmental alterations and autophagy activity progression. Notably, recent research reveals that HSP60 can directly bind to LC3B, acting as an 'eat-me' signal for mitophagy [33]. In this study, we observed that silencing the NLRX1 gene led to an abnormal increase in HSP60 levels, while NLRX1 overexpression significantly reduced its expression. This phenomenon may involve a dual mechanism: (1) Enhanced autophagic clearance: NLRX1 selectively clears pathological mitochondria with high HSP60 expression through promoting mitophagy, reducing overall HSP60 burden. A similar mechanism has been reported in Parkinson's disease models; (2) Oxidative stress relief: NLRX1 reduces mitochondrial oxidative damage by inhibiting ROS production, decreasing misfolded protein generation, and thus lowering HSP60 chaperone demand. Recent studies suggest that NLRX1 May regulate mitophagy via the PINK1/Parkin pathway [34]. In our study, co-immunoprecipitation assays in N2A-SW cells further revealed that NLRX1 interacts with key mitophagy-related proteins, including PINK1, Parkin, LC3B, and HSP60. Cyt-C is one of the important molecules for maintaining mitochondrial quality control and cellular homeostasis within the neuron [35]. These findings suggest that NLRX1 May orchestrate mitophagy through both signaling regulation and protein – protein interactions, offering new insights into mitochondrial quality control in Alzheimer's disease.

This study has several limitation that warrant consideration. First, the causal relationship between NLRX1, mitophagy, and Aβ remains incompletely defined: while we show correlations, experiments using NLRX1 knockout mice crossed with APP/PS1 models would clarify whether NLRX1 deletion accelerates AD pathology in vivo. Additionally, the use of APP/PS1 mice and N2A-SW cells, while informative, may not completely replicate all aspects of human Alzheimer's disease pathology. Future studies involving more complex models and clinical samples will be necessary for a comprehensive understanding of these mechanisms. Due to the lack of an automated tracking system for Y-maze, trajectory data (heatmaps or path traces) were not available. All sessions of Y-maze experiment were video-recorded, and alternation behavior was manually scored by trained observers blinded to group assignment. In summary, NLRX1, a mitochondria-localized NOD-like receptor, plays a pivotal role in regulating the process of AD mitophagy. Our findings align with the established role of NLRX1 as a positive regulator of mitophagy: NLRX1 overexpression enhanced autophagosome formation (evidenced by an increased LC3B-II/I ratio) and improved mitochondrial health, whereas NLRX1 knockdown exacerbated mitochondrial damage and suppressed mitophagic markers. This consistency underscores the protective function of NLRX1 in maintaining mitochondrial homeostasis, as observed in other pathological models. Therefore, the study of NLRX1 will provide a new perspective for the study of the pathological mechanisms of AD and the exploration of therapeutic targets.

Acknowledgments

We'd like to thank Huiling Gao from Northeastern University, N2A-SW cells.

Disclosure statement

No potential conflict of interest was reported by the author(s).

Funding

This study was supported by the Basic Research Project of Liaoning Provincial Department of Education [LJKMZ20221804], the Basic Research Project of Liaoning Provincial Department of Education [LJ212410164005], the Science and Technology Foundation Project of Shenyang Medical College [20203038] and the College Students' Innovation and Entrepreneurship Training Program [202310164005].

ORCID

Ling Xie http://orcid.org/0009-0004-1612-5702

References

[1] Scheltens P, De Strooper B, Kivipelto M, et al. Alzheimer's disease. Lancet. 2021;397(10284):1577–1590. doi: 10.1016/S0140-6736(20)32205-4
[2] Livingston G, Huntley J, Sommerlad A, et al. Dementia prevention, intervention, and care: 2020 report of the Lancet Commission. Lancet. 2020;396(10248):413–446. doi: 10.1016/S0140-6736(20)30367-6
[3] van den Brink AC, Brouwer-Brolsma EM, Berendsen AAM, et al. The Mediterranean, dietary approaches to stop hypertension (DASH), and Mediterranean-DASH intervention for neurodegenerative delay (MIND) diets are associated with less cognitive decline and a lower risk of Alzheimer's disease-a review. Adv Nutr. 2019;10(6):1040–1065. doi: 10.1093/advances/nmz054
[4] Picard M, Shirihai OS. Mitochondrial signal transduction. Cell Metab. 2022;34(11):1620–1653. doi: 10.1016/j.cmet.2022.10.008
[5] Ashleigh T, Swerdlow RH, Beal MF. The role of mitochondrial dysfunction in Alzheimer's disease pathogenesis. Alzheimers DeMent. 2023;19(1):333–342, doi: 10.1002/alz.12683
[6] Maria Clara Bila DA, Salim K, Mauro G, et al. Mitochondrial dysfunction in Alzheimer's disease. Ageing Res Rev. 2025;107:102713. doi: 10.1016/j.arr.2025.102713
[7] Rosenberg A, Mangialasche F, Ngandu T, et al. Multidomain interventions to prevent cognitive impairment, Alzheimer's disease, and dementia: from FINGER to world-wide FINGERS. J Prev Alzheimers Dis. 2020;7(1):29–36. doi: 10.14283/jpad.2019.41

[8] Bock FJ, Tait SWG. Mitochondria as multifaceted regulators of cell death. Nat Rev Mol Cell Biol. 2020;21 (2):85–100. doi: 10.1038/s41580-019-0173-8
[9] Nikolaos C, Evandro Fei F, Konstantinos PJCN. Mitophagy and neuroinflammation: a compelling interplay. Curr Neuropharmacol. 2022;21. doi: 10.2174/1570159x20666220628153632
[10] Kuan Z, Yu X, Mahaman YAR, et al. Defective mitophagy and the etiopathogenesis of Alzheimer's disease. Transl NeurodeGener. 2022;11(1). doi: 10.1186/s40035-022-00305-1
[11] Ela M, Mahendra Kumar TJB. Alterations in hippocampal mitochondrial dynamics are associated with neurodegeneration and recognition memory decline in old male mice. Biogerontology. 2022;23(2):251–271. doi: 10.1007/s10522-022-09960-3
[12] Evandro FF, Yujun H, Konstantinos P, et al. Mitophagy inhibits amyloid-β and tau pathology and reverses cognitive deficits in models of Alzheimer's disease. Nat Neurosci. 2019;22. doi: 10.1038/s41593-018-0332-9
[13] Hroudova J, Singh N, Fisar Z. Mitochondrial dysfunctions in neurodegenerative diseases: relevance to Alzheimer's disease. Biomed Res Int. 2014;2014:175062, doi: 10.1155/2014/175062
[14] Cunnane SC, Trushina E, Morland C, et al. Brain energy rescue: an emerging therapeutic concept for neurodegenerative disorders of ageing. Nat Rev Drug Discov. 2020;19(9):609–633. doi: 10.1038/s41573-020-0072-x
[15] Butterfield DA, Halliwell B. Oxidative stress, dysfunctional glucose metabolism and Alzheimer disease. Nat Rev neurosci. 2019;20(3):148–160. doi: 10.1038/s41583-019-0132-6
[16] Chen L, Cao SQ, Lin ZM, et al. Nod-like receptors in autoimmune diseases. Acta Pharmacol sin. 2021;42 (11):1742–1756. doi: 10.1038/s41401-020-00603-2
[17] Rebecca R, Bolmont T, Kaeser SA, et al. Abeta42-driven cerebral amyloidosis in transgenic mice reveals early and robust pathology. EMBO Rep. 2006;7(9). doi: 10.1038/sj.embor.7400784
[18] Adrian LO, Stefania F, Paul RT, et al. Model organism development and evaluation for late-onset Alzheimer's disease. Model-Ad. 2020;6. doi: 10.1002/trc2.12110
[19] Yuzhi C, Wenyun L, Donna L, et al. App-bp1 mediates APP-induced apoptosis and DNA synthesis and is increased in Alzheimer's disease brain. J Cell Biol. 2003;163(1):27–33. doi: 10.1083/jcb.200304003
[20] Pradeepkiran JA, Reddy PH. Defective mitophagy in Alzheimer's disease. Ageing Res Rev. 2020;64:101191. doi: 10.1016/j.arr.2020.101191
[21] Knopman DS, Amieva H, Petersen RC, et al. Alzheimer disease. Nat Rev Dis Primers. 2021;7(1):33. doi: 10.1038/s41572-021-00269-y
[22] Yu JT, Xu W, Tan C-C, et al. Evidence-based prevention of Alzheimer's disease: systematic review and meta-analysis of 243 observational prospective studies and 153 randomised controlled trials. J Neurol Neurosurg Psychiatry. 2020;91(11):1201–1209. doi: 10.1136/jnnp-2019-321913
[23] Arnaud M, Fanny E, Frédéric C, et al. Mitophagy in Alzheimer's disease: molecular defects and therapeutic approaches. Mol Psychiatry. 2022;28(1):202–216. doi: 10.1038/s41380-022-01631-6
[24] Tattoli I, Killackey S, Foerster E, et al. Nlrx1 acts as an epithelial-intrinsic tumor suppressor through the modulation of TNF-mediated proliferation. Cell Rep. 2016;14(11):2576–2586. doi: 10.1016/j.celrep.2016.02.065
[25] Ding Y, Sun W, Han M, et al. Nlrx1: a key regulator in mitochondrial respiration and colorectal cancer progression. Med Oncol. 2024;41(6):131. doi: 10.1007/s12032-024-02364-y
[26] Pickering RJ, Booty LM. Nlr in exile: emerging roles of NLRX1 in immunity and human disease. Immunology. 2021;162(3):268–280, doi: 10.1111/imm.13291
[27] Chu X, Wu S, Raju R. Nlrx1 regulation following acute mitochondrial injury. Front Immunol. 2019;10:2431. doi: 10.3389/fimmu.2019.02431
[28] Killackey SA, Bi Y, Soares F, et al. Mitochondrial protein import stress regulates the LC3 lipidation step of mitophagy through NLRX1 and RRBP1. Mol Cell. 2022;82(15):2815–2831 e2815. doi: 10.1016/j.molcel.2022.06.004
[29] Eiyama A, Okamoto K. Ink1/Parkin-mediated mitophagy in mammalian cells. Curr Opin Cell Biol. 2015;33:95–101, doi: 10.1016/j.ceb.2015.01.002
[30] Chacinska A, Koehler CM, Milenkovic D, et al. Importing mitochondrial proteins: machineries and mechanisms. Cell. 2009;138(4):628–644. doi: 10.1016/j.cell.2009.08.005
[31] Wiedemann N, Pfanner N. Mitochondrial machineries for protein import and assembly. Annu Rev Biochem. 2017;86(1):685–714. doi: 10.1146/annurev-biochem-060815-014352
[32] Rugarli EI, Langer T. Mitochondrial quality control: a matter of life and death for neurons. Embo J. 2012;31 (6):1336–1349. doi: 10.1038/emboj.2012.38
[33] Pickles S, Vigie P, Youle RJ. Mitophagy and quality control mechanisms in mitochondrial maintenance. Curr Biol. 2018;28(4):R170–R185. doi: 10.1016/j.cub.2018.01.004
[34] Lixin Y, Qiao P, Li X, et al. Nlrx1 deficiency exacerbates skin inflammation in atopic dermatitis by disrupting mitophagy. Clin Immunol. 2025;272:110442. doi: 10.1016/j.clim.2025.110442
[35] Li X, Wang C, Zhu J, et al. Sodium butyrate ameliorates oxidative stress-induced intestinal epithelium barrier injury and mitochondrial damage through AMPK-mitophagy pathway. Oxid Med Cell Longev. 2022;2022 (1):3745135. doi: 10.1155/2022/3745135